A Journal of the Gesellschaft Deutscher Chemiker
Angewandte Chemie
GDCh
International Edition
www.angewandte.org

Accepted Article

Title: Synthesis of Boron-imidazolate Framework nanosheet with Dimer Cu units for CO2 Electroreduction to Ethylene

Authors: Ping Shao, Wei Zhou, Qin-Long Hong, Luocai Yi, Lirong Zheng, Wenjing Wang, Hai-Xia Zhang, Huabin Zhang, and Jian Zhang

To be cited as: *Angew. Chem. Int. Ed.* 10.1002/anie.202106004

Link to VoR: https://doi.org/10.1002/anie.202106004

WILEY-VCH

RESEARCH ARTICLE WILEY-VCH

Synthesis of a Boron-Imidazolate Framework Nanosheet with Dimer Cu Units for CO_2 Electroreduction to Ethylene

Ping Shao,†[a] Wei Zhou,†[b] Qin-Long Hong,[a] Luocai Yi,[a] Lirong Zheng,[d] Wenjing Wang,[a] and Hai-Xia Zhang,*[a] Huabin Zhang,[c] Jian Zhang*[a]

[a] P. Shao, Q.-L. Hong, L Yi, Dr. W. Wang, and Prof. H.-X. Zhang, Prof. J. Zhang
State Key Laboratory of Structural Chemistry, Fujian Institute of Research on the Structure of Matter
Chinese Academy of Sciences
Fuzhou, Fujian 350002, P. R. China
E-mail: Zhanghaixia@fjirsm.ac.cn; zhj@fjirsm.ac.cn.

[b] Dr. W. Zhou
Department of Applied Physics, Tianjin Key Laboratory of Low Dimensional Materials Physics and Preparing Technology, Faculty of Science
Tianjin University
Tianjin 300072, P. R. China

[c] Prof. H. Zhang
KAUST Catalysis Center (KCC)
King Abdullah University of Science and Technology (KAUST)
Thuwal 23955-6900, Saudi Arabia

[d] Prof. L. Zheng
Beijing Synchrotron Radiation Facility, Institute of High Energy Physics
Chinese Academy of Sciences
No. 19 Yuquan Road, Beijing 100049, China

† These authors contributed equally to this work.

Supporting information for this article is given via a link at the end of the document.

Abstract: Fundamental understanding of the dependence between the structure and composition on the electrochemical CO_2 reduction reaction (CO_2RR) would guide the rational design of highly efficient and selective electrocatalysts. A major impediment to the deep reduction CO_2 to multi-carbon products is the complexity of carbon-carbon bond coupling. The chemically well-defined catalysts with atomically dispersed dual-metal sites are required for these C-C coupling involved processes. Here, we developed a catalyst (BIF-102NSs) that features Cl^- bridged dimer copper (Cu_2) units, which delivers high catalytic activity and selectivity for C_2H_4. Mechanistic investigation verifies that neighboring Cu monomers not only perform as regulator for varying the reaction barrier, but also afford distinct reaction paths compared with isolated monomers, resulting in greatly improved electroreduction performance for CO_2.

Introduction

The electrochemical conversion of CO_2 and water into fuels and chemicals, ideally if driven by renewable energy, holds great promise to alleviate the depletion of fossil resources and reduce the carbon emission.[1] As CO_2 is a thermodynamically stable and kinetically inert molecule, the electrochemical CO_2 reduction reaction (CO_2RR) is a process that requires high energy input.[2] To date, numerous efficient electrocatalysts for converting CO_2 into C_1 products (carbon monoxide, methane and formic acid) have been reported with high Faradaic efficiency and selectivity.[3] Comparing with C_1 products, C_2 and C_{2+} species (ethylene, ethanol, propane, *etc.*) are especially attractive because of their higher volumetric energy densities and broader applications. However, due to the higher kinetic barrier in the C-C coupling process, producing multi-carbon hydrocarbons and oxygenates is a big challenge for the CO_2RR.[4]

As one holy grail in the synthesis science, construction of catalysts at molecular scale can lead to extremely high atom utilization and exceptional catalytic performance, especially provide mechanistic insight into catalytic process.[5] Currently, Cu-based materials are the most selective catalysts for electrocatalytic CO_2RR to deeply reduced C_{2+} products. Although high activities of multi-carbon products have been obtained by tailoring strategies on Cu-based catalysts, such as morphology and facet controlling,[6] size tuning,[7] defect engineering and dopant modification,[8] the formation mechanism for C_{2+} species has not been fully resolved.[9] For the most accepted one, the C-C formation step through *CO dimerization or coupling pathway is regarded as the rate-determining step.[10] To improve the formation of multi-carbon products, the precursor of the adsorbed CO (*CO) on the surface should be present in close proximity to one another. This requires specific dual-metal sites in the catalyst, which may produce synergistic effect on two adjacent sites to facilitate the C-C bond coupling. However, by downsizing the metal nanoparticles for fabrication of dimer-copper catalysts remains a significant challenge. Therefore, it is meaningful to synthesize dimer-copper catalysts with well-defined structures as a model electrocatalyst for the studies of CO_2RR.

Metal−organic frameworks (MOFs), constructed by metal nodes and organic ligands, are a class of distinctive crystalline materials with precise spatial arrangement of metal atoms.[11] Owing to their structural adjustability, MOFs can offer a highly versatile platform for catalysis.[12] However, the reaction condition for CO_2RR is somewhat harsh, and most of the reported MOFs can hardly maintain pristine crystallinities during the reaction process. An effective strategy to improve the chemical stability of MOFs is to construct robust metal-ligand coordinate bonds by using basic N-donor ligands, such as azolate ligands.[11a] Boron imidazolate frameworks (BIFs) are one kind of azolate-based MOFs constructed by the crosslinking of metal ions and boron imidazolate ligands.[13] Because of the presence of robust M-N coordination bonds, together with the

strong covalent bonds (B-N), BIFs hold promise for the development of chemical stable crystalline catalysts for CO_2RR. Additionally, predesigned boron imidazolate ligands provide room for adjusting the microenvironments around the active centers. Recent studies demonstrated that introducing isolated square-planar Cu site in BIF can stabilize the reaction intermediates and improve the activity for CO_2 photoreduction.[13c] Besides this, introducing bimetallic Cu sites in catalysts can alter the adsorption energy barrier of reaction intermediates over active sites and promote C–C coupling for CO_2 reduction reaction.[7a]

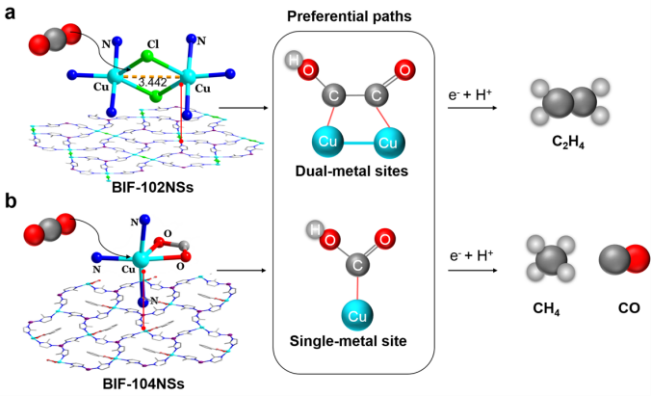

Figure 1. Coordination environment of BIF-102NSs and BIF-104NSs and the illustration showing the preferential reaction pathways of different model systems**.**

With these considerations, we have successfully elaborated dimer-copper catalysts $Cu(II)_2[BH(mim)_3]_2Cl_2$ (BIF-102, mim = 2-methylimidazole) and $Cu(II)_2$ $[BH(mim)_3]_2(HCOO)_2$ (BIF-103) with varied bridging ligands. For reference, catalyst $Cu(II)_2[BH(mim)_3]_2(BA)_2$ (BIF-104, BA = benzoate) with isolated Cu sites has also been developed (Figure 1 and Figure S2).[17] Electrocatalytic results clearly demonstrated that the dimer-copper sites with the cooperative nature could deliver efficient faradic efficiency (FE) for the generation of C_2H_4 product. Furthermore, the Cl^- ions bridged BIF-102NSs shows better performance with higher selectivity for C_2H_4. This work suggests that modulating the coordination environment of metal centers is one way to tailor the product selectivity of CO_2RR, providing insights into the influence of different metal clusters on CO_2RR.

Results and Discussion

As depicted in Figure S1, bulk crystals of BIF-102, BIF-103, and BIF-104 were firstly synthesized under solvothermal condition by reacting $BH(mim)_3^-$ with different copper salts. Then, the as-prepared bulk crystals were dispersed in ethanol and exfoliated by ultrasonication, resulting in the formation nanosheets (noted as BIF-102NSs, BIF-103NSs, and BIF-104NSs). Single-crystal X-ray diffraction analysis revealed that all of them have 2D layer frameworks. BIF-102 and BIF-103 have almost identical host frameworks which contain binuclear Cu_2 as metal nodes further connected by six $BH(mim)_3^-$ ligands (Figure S2a-b). In both structures, Cu ions adopt the five-coordinated triangular bipyramid modes in which three N atoms from three $BH(mim)_3^-$ ligands. The only difference is that the Cu_2 node is bridged by two μ_2-bridging Cl^- ions in BIF-102, while Cu_2 node is bridged by one μ_2-bridging O from COO^- and one bridging η^2-COO^- in BIF-103 (Figure 1 and S2). Unlike BIF-102 and BIF-103, BIF-104 contains mononuclear Cu ions as metal nodes linked by three $BH(mim)_3^-$ ligands to form a 2D layer (Figure S2c and f). Cu ions in BIF-104 also adopt the five-coordinated triangular bipyramid modes with three N atoms from three $BH(mim)_3^-$ ligands and two O atoms from chelating carboxylate of the pendent auxiliary benzoic acid ligand (Figure 1b). The powder X-ray diffraction (PXRD) investigations showed that both the as-synthesized bulk crystals and the exfoliated nanosheets matched well with the simulated one from the crystal structures, indicating that the crystal structures of BIF-102, BIF-103 and BIF-104 were well retained (Figure S2g-i). Furthermore, all these samples can maintain their structural integrity after soaking in acidic/basic ($1 \leq pH \leq 12$) aqueous solutions, indicating the extraordinary chemical stability of boron imidazolate frameworks (Figure S22-S24).

Ultrathin nanosheets morphology of the as-synthesized hybrids can be discerned well by transmission electron microscopy (TEM), atomic force microscopy (AFM) (Figure 2, S3, and S4). The nearly transparent feature of the BIF-102NSs demonstrates their ultrathin thickness (Figure 2 a-b). Energy dispersive spectroscopy (EDS) measurement indicates that BIF-102NSs electrocatalysts contain Cu, Cl, C, and N, without other impurities (Table S1). Element mapping on these nanosheets also confirms these elements are uniformly distributed throughout entire BIF-102NSs (Figure 2c-d). AFM offers more detailed information of these nanosheets. As shown in Figure 2e and f, the exfoliated BIF-102NSs display uniform thickness of about 1.2 nm. Benefitting from the ultrathin nanosheets of the 2D layered structure; these catalysts may expose more active sites for improving efficient catalytic activity in electrocatalytic reduction of CO_2.

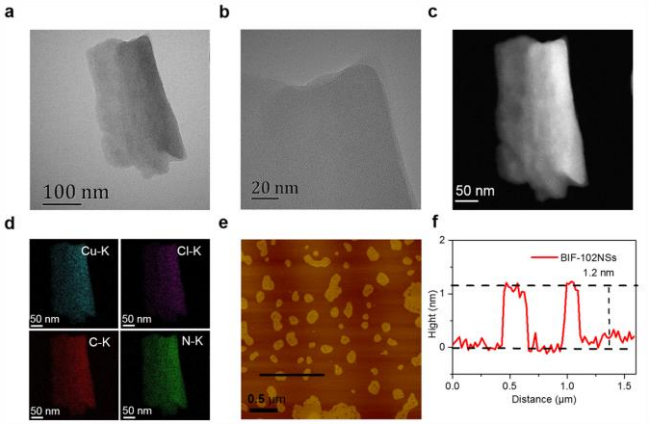

Figure 2. a) TEM and b) HRTEM image of BIF-102NSs electrocatalysts; c) High-angle annular dark-field (HAADF) STEM image and d) corresponding mapping of Cu, Cl, C and N in BIF-102NSs; e) AFM image and f) corresponding height of as-synthesized BIF-102NSs.

For gain more accurate structural information about the chemical status and elemental composition of the samples, X-ray absorption near-edge structure (XANES) and X-ray photoelectron spectra (XPS) are performed. As shown in XANES (Figure 3a), the absorption edges of BIF-102NSs, BIF-103NSs and BIF-104NSs are clearly presented with nearly

identical profiles. The absorption edge positions are comparable to that of CuO, suggesting the divalent state of Cu ions in the three electrocatalysts.[8b,14] The XPS survey scans clearly display the presence of B, C, N, and Cu in BIF-102NSs, BIF-103NSs and BIF-104NSs. Moreover, the existence of Cl is also detected in BIF-102NSs (Figure S5a-c). The Cl 2*p* spectrum for BIF-102NSs shows the main peaks at 199.1 eV, which should be assigned to Cl^- anion (Figure 3b).[15] The N 1*s* spectra of all three samples are quite similar and deconvoluted into two peaks centered at 398.8 and 399.7 eV, corresponding to the N-B and N-Cu bonding, respectively (Figure 3c).[5e, 12b] The high-resolution XPS Cu 2*p* spectra of the samples display the dominant peak of about 934.6 eV, closing to that of Cu^{2+} compounds with N ligands (Figure 3d).[16]

To elucidate the electrocatalytic performances, cyclic voltammograms (CV) and linear sweep voltammograms (LSV) curves are measured from 0 to −1.0 V versus reversible hydrogen electrode (vs. RHE) in both CO_2 and Ar saturated 0.5 M $KHCO_3$ electrolyte (Figure S6, S7). The greater current density and more positive onset potential in CO_2 saturated solution for each sample demonstrated that the three BIFs show possibly favorable activity toward CO_2RR compared with hydrogen evolution reaction (HER). As revealed by LSV in Figure 4a, BIF-102NSs displayed the most positive onset potential of -0.51 V and the highest total current density at potential from -0.60 V to 0.96 V when comparing with BIF-103NSs and BIF-104NSs. BIF-102NSs exhibited a current density of 12.1 mA cm^{-2} at 0.94 V, which is about 2.08 and 3.1 times larger than that for BIF-103NSs (5.8 mA cm^{-2}) and BIF-104NSs (3.9 mA cm^{-2}) at the identical operation voltage, respectively.

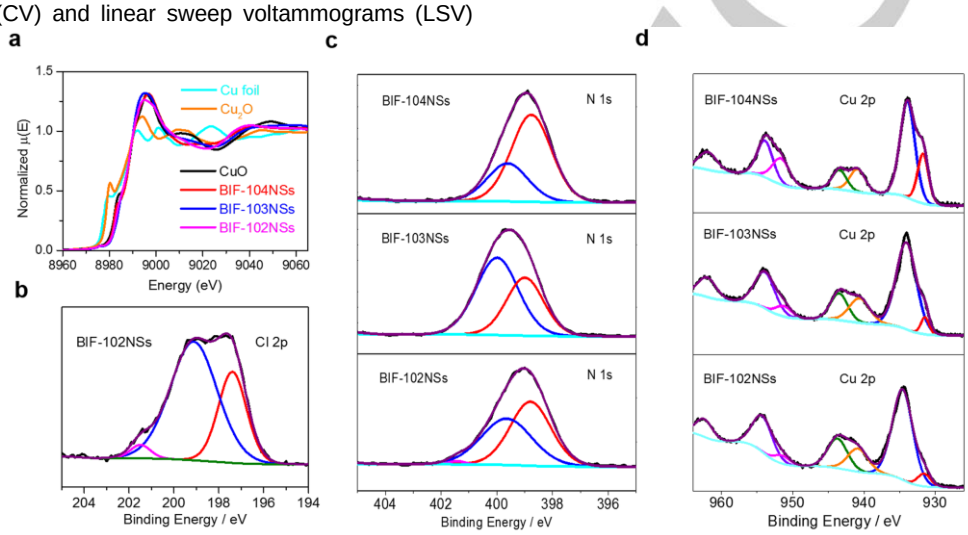

Figure 3. a) XANES spectra at the Cu K-edge of the BIF-102NSs, BIF-103NSs, BIF-104NSs, Cu foil, Cu_2O, and CuO; b) Cl 2p XPS spectrum of BIF-102NSs; c) N 1s spectra and d) Cu 2p spectra of BIF-102NSs, BIF-103NSs, and BIF-104NSs.

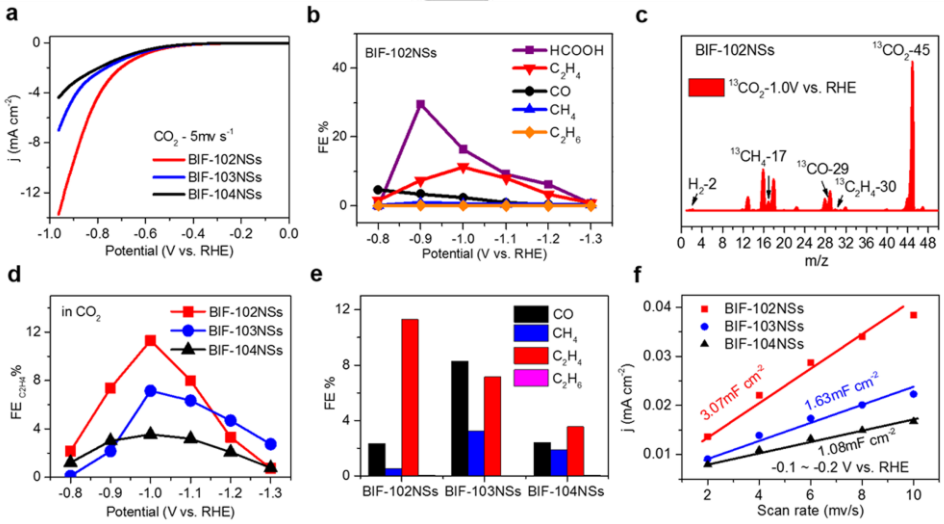

Figure 4. a) LSV curves of BIF-102NSs, BIF-103NSs, and BIF-104NSs electrocatalysts in CO_2 saturated 0.5 M $KHCO_3$ electrolyte, respectively; b) The FE of valuable gas and liquid products of BIF-102NSs electrocatalysts at different applied potentials in CO_2 saturated electrolyte; c) Mass spectrum of gases from the electrocatalytic reduction of $^{13}CO_2$ with BIF-102NSs as electrocatalysts; d) The FE_{C2H4} of BIF-102NSs, BIF-103NSs, and BIF-104NSs electrocatalysts at different applied potentials in CO_2 saturated electrolyte; e) Comparison of the CO_2RR gas productions activity between BIF-102NSs, BIF-103NSs, and BIF-104NSs electrocatalysts at -1.0 V vs. RHE in CO_2 saturated electrolyte; f) The C_{dl} of BIF-102NSs, BIF-103NSs, and BIF-104NSs electrocatalysts.

Electrolysis at fixed potentials are further performed to monitor the products of CO_2 reduction by gas chromatography (GC) and ^1H nuclear magnetic resonance (NMR) spectroscopy. The detected gas-phase products involve CO, CH_4, C_2H_4, and a trace amount of C_2H_6. Besides, the liquid-phase products of HCOOH is also monitored in all those catalytic processes. The generated products are highly relevant to the operation electrode potentials (Figure S8, S9, and S10). Major product of HCOOH with the highest Faradaic efficiency (FE) of 29.58% is detected over BIF-102NSs at lower overpotentials (Figure S8c). With the negative shifting of electrode potential, FE_{HCOOH} decreases gradually while C_2H_4 becomes the dominant CO_2 reduction product. The FE_{C2H4} significantly increases as potential shifted from -0.8 V to -1.0 V and achieved 11.30% at -1.0 V, which is much higher than those of FE calculated from the CO, CH_4, and C_2H_6 production (Figure 4b). However, hydrogen evolution reaction (HER) become more competitive at more negative potentials, the FE of valuable products gradually decrease while FE of H_2 increase. In addition, Ar instead of CO_2 is also introduced into the same reaction system to reveal the origin of the products and only H_2 was detected (Table S2). The $^{13}CO_2$ isotopic investigation is further conducted for confirming the origin of the products. As shown in Figure 4c, the peak of m/z = 30 assigning to the $^{13}C_2H_4$ is clearly presented, further demonstrating that the carbon source of C_2H_4 originates from the introduced CO_2. Electrocatalytic stability for the BIF-102NSs is also characterized by using chronoamperometric and related FE_{C2H4} curves. At the applied potential of -1.0 V, BIF-102NSs exhibited no obvious degradation of current density and the faradaic efficiency of C_2H_4 during after electrolyzing 5 h at -1.0 V (Figure S11).

Comparisons for the catalytic performances among BIF-102NSs, BIF-103NSs and BIF-104NSs are also conducted (Figure 4d and 4e). As observed, BIF-102NSs and BIF-103NSs with binuclear Cu_2 units exhibit superior activity and selectivity for C_2 hydrocarbons (C_2H_4) than that of BIF-104NSs with isolated Cu sites, demonstrating that the binuclear Cu_2 units work as promoter in the evolution of C_2 products. Moreover, BIF-102NSs deliver better performance than that of BIF-103NSs in the evolution of C_2H_4. This fact should be attributed to the chlorine bridges in BIF-102NSs induced modulating effects between the binuclear Cu_2 units. Correspondingly, electrochemical double-layer capacitances (C_{dl}) are calculated from CV curves to estimate the electrochemical active surface area (Figure 4f and S12). BIF-102NSs exhibit the largest C_{dl} value (3.07 mF cm^{-2}) than those of BIF-103NSs (1.63 mF cm^{-2}) and BIF-104NSs (1.08 mF cm^{-2}), demonstrating that BIF-102NSs provide more active sites being beneficial to CO_2 electroreduction reaction. Moreover, the electrochemical impedance spectroscopy (EIS) (Figure S13) also indicates that BIF-102NSs exhibit the smallest curvature radius of the semicircular Nyquist plots. The tafel plot of the logarithm values of current density (log j) against overpotential demonstrated that the BIF-102NSs exhibited the smallest Tafel slope (Figure S14). These results implied that the BIF-102NSs has highest charge transfer efficiency when comparing with those of BIF-103NSs and BIF-104NSs.

To unveil the effects of dimer-copper units and atomic configuration on the reaction mechanism of CO_2RR, density-functional theory (DFT) simulations are performed. Figure 5a shows the density of states (DOS) of BIF-102, BIF-103 and BIF-104. Comparing with the mononuclear structure of BIF-104, the existences of binuclear Cu_2 units in BIF-102 and BIF-103 structures obviously weaken the electronic states in the vicinity of the Fermi level, resulting in much weaken interactions between the CO_2 molecular and reactive centers. Furthermore, comparing with BIF-103, some new enhanced hybridized electronic states appear in BIF-102, as observed from the calculated projected density of state (PDOS) of Cu atoms (Figure 5b). The emergence of new electronic states could be attributed to the existence of Cl species in BIF-102 with higher electronegativity, which may also weaken the binding between CO_2 molecules and copper clusters and result in a moderate adsorption energy. In another hand, as the C-C coupling is a key step in the formation of C_2H_4 products, moderate adsorption is a critical property to the further coupling between the CO_2 molecules from the adjacent Cu sites, realizing the C-C coupling in an efficient way. The adsorption free energy (E_0) of CO_2 is also investigated. The binding of CO_2 is energetically favored on all the three catalysts, as evidenced by these negative values (Figure 5c). The binding forces of BIF-102 is moderate, which is weaker than both BIF-103 and BIF-104. Corresponding distribution of charge densities has also been investigated, further proving that the coupling of CO_2 molecules around the copper cluster of BIF-102 is easier than that of BIF-103 and BIF-104 (Figure 5d).

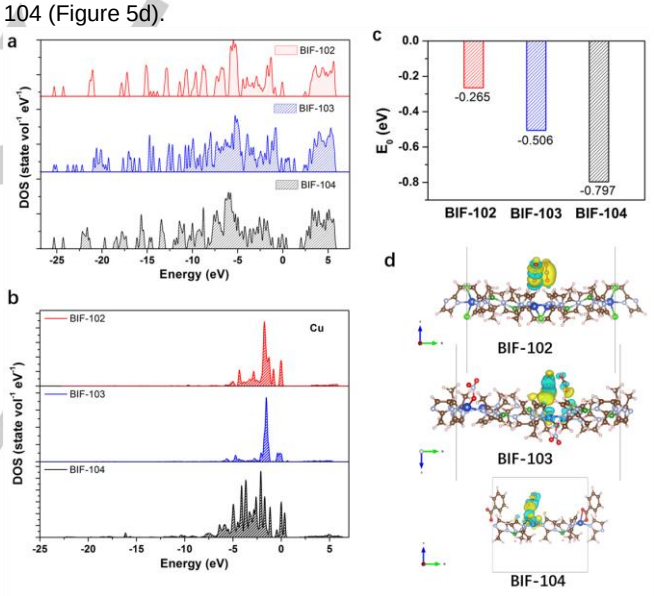

Figure 5. DFT calculation results. Calculated TDOS a) and PDOS-Cu b) of BIF-102, BIF-103 and BIF-104; c) the adsorption free energy of CO_2 at BIF-102, BIF-103 and BIF-104; d) Calculated distribution of charge density of BIF-102, BIF-103 and BIF-104.

Conclusion

In this work, we constructed a dual-copper site that is anchored on ultrathin boron imidazolate layers (BIF-102NSs) to tailor the reactivity and selectivity of CO_2 electroreduction reaction. Electrocatalytic results clearly demonstrated that BIF-102NSs could efficiently enhance the faradic efficiency of C_2H_4 products (FE of 11.3%), which is 1.6-fold enhancements of its iso-reticular counterparts (BIF-103 FE of 7.15%) and 3.2-fold enhancements of its single-metal counterparts (BIF-104 FE of 3.55%). Based on the X-ray absorption near-edge structure (XANES), X-ray photoelectron spectra (XPS), and

electrochemical kinetics analysis, we attributed the enhanced performance to the cooperative nature of the dual-metal sites resulting in charge enrichment on the surrounding Cu centers. Our findings point out a new avenue to modulate the synergetic interaction between neighbouring monomers for varying the reaction path of CO_2 electroreduction advancing further comprehension for the C-C coupling in the CO_2 reduction process.

Acknowledgements

This work is supported by National Natural Science Foundation of China (21935010, 21773242), National Key Research and Development Program of China (2018YFA0208600), and the Strategic Priority Research Program of the Chinese Academy of Sciences (XDB20000000).

Keywords: CO_2 reduction • electrocatalysis • crystal • metal-organic framework • catalyst

[1] a) R. M. Arán-Ais, D. Gao, B. Roldan Cuenya, *Acc. Chem. Res.* **2018**, *51*, 2906-2917; b) M. B. Ross, P. De Luna, Y. Li, C.-T. Dinh, D. Kim, P. Yang, E. H. Sargent, *Nat. Catal.* **2019**, *2*, 648-658; c) D. D. Zhu, J. L. Liu, S. Z. Qiao, *Adv. Mater.* **2016**, *28*, 3423-3452.

[2] a) S. Xu, E. A. Carter, *Chem. Rev.* **2019**, *119*, 6631-6669; b) M. G. Kibria, J. P. Edwards, C. M. Gabardo, C. T. Dinh, A. Seifitokaldani, D. Sinton, E. H. Sargent, *Adv. Mater.* **2019**, *31*, 1807166; c) K. Elouarzaki, V. Kannan, V. Jose, H. S. Sabharwal, J. M. Lee, *Adv. Energy Mater.* **2019**, *9*, 1900090; d) Y. Sun, S. Gao, Y. Xie, *Chem. Soc. Rev.* **2014**, *43*, 530-546; e) Y. Zheng, A. Vasileff, X. Zhou, Y. Jiao, M. Jaroniec, S.-Z. Qiao, *J. Am. Chem. Soc.* **2019**, *141*, 7646-7659; f) W. Luc, X. Fu, J. Shi, J.-J. Lv, M. Jouny, B. H. Ko, Y. Xu, Q. Tu, X. Hu, J. Wu, Q. Yue, Y. Liu, F. Jiao, Y. Kang, *Nat. Catal.* **2019**, *2*, 423-430; g) Q. Lu, F. Jiao, *Nano Energy* **2016**, *29*, 439-456.

[3] a) H.-J. Zhu, M. Lu, Y.-R. Wang, S.-J. Yao, M. Zhang, Y.-H. Kan, J. Liu, Y. Chen, S.-L. Li, Y.-Q. Lan, *Nat. Commun.* **2020**, *11,* 497; b) E. Zhang, T. Wang, K. Yu, J. Liu, W. Chen, A. Li, H. Rong, R. Lin, S. Ji, X. Zheng, Y. Wang, L. Zheng, C. Chen, D. Wang, J. Zhang, Y. Li, *J. Am. Chem. Soc.* **2019**, *141*, 16569-16573; c) Z. Weng, Y. Wu, M. Wang, J. Jiang, K. Yang, S. Huo, X.-F. Wang, Q. Ma, G. W. Brudvig, V. S. Batista, Y. Liang, Z. Feng, H. Wang, *Nat. Commun.* **2018**, *9,* 415; d) R. Matheu, E. Gutierrez-Puebla, M. Á. Monge, C. S. Diercks, J. Kang, M. S. Prévot, X. Pei, N. Hanikel, B. Zhang, P. Yang, O. M. Yaghi, *J. Am. Chem. Soc.* **2019**, *141*, 17081-17085; e) L. Lin, H. Li, C. Yan, H. Li, R. Si, M. Li, J. Xiao, G. Wang, X. Bao, *Adv. Mater.* **2019**, *31*, 1903470; f) H. Yang, Y. Wu, G. Li, Q. Lin, Q. Hu, Q. Zhang, J. Liu, C. He, *J. Am. Chem. Soc.* **2019**, *141*, 12717-12723; g) Y. Wang, J. Chen, G. Wang, Y. Li, Z. Wen, *Angew. Chem. Int. Ed.* **2018**, *57*, 13120-13124; h) J. Choi, P. Wagner, S. Gambhir, R. Jalili, D. R. MacFarlane, G. G. Wallace, D. L. Officer, *ACS Energy Lett.* **2019**, *4*, 666-672; i) M. Kuang, A. Guan, Z. Gu, P. Han, L. Qian, G. Zheng, *Nano Res.* **2019**, *12*, 2324-2329; j) S. Mou, T. Wu, J. Xie, Y. Zhang, L. Ji, H. Huang, T. Wang, Y. Luo, X. Xiong, B. Tang, X. Sun, *Adv. Mater.* **2019**, *31*, 1903499; k) H. Yang, Y. w. Hu, J. j. Chen, M. S. Balogun, P. P. Fang, S. Zhang, J. Chen, Y. Tong, *Adv. Energy Mater.* **2019**, *9*, 1901396; l) X. Li, Y. Sun, J. Xu, Y. Shao, J. Wu, X. Xu, Y. Pan, H. Ju, J. Zhu, Y. Xie, *Nat. Energy* **2019**, *4*, 690-699; m) J. Fu, W. Zhu, Y. Chen, Z. Yin, Y. Li, J. Liu, H. Zhang, J. J. Zhu, S. Sun, *Angew. Chem. Int. Ed.* **2019**, *58*, 14100-14103.

[4] a) D. Ren, B. S.-H. Ang, B. S. Yeo, *ACS Catal.* **2016**, *6*, 8239-8247; b) A. A. Peterson, F. Abild-Pedersen, F. Studt, J. Rossmeisl, J. K. Nørskov, *Energy Environ. Sci.* **2010**, *3*, 1311; c) W. Bi, C. Wu, Y. Xie, *ACS Energy Lett.* **2018**, *3*, 624-633; d) K. D. Yang, C. W. Lee, K. Jin, S. W. Im, K. T. Nam, *J. Phys. Chem. Lett.* **2017**, *8*, 538-545.

[5] a) J. Jiao, R. Lin, S. Liu, W.-C. Cheong, C. Zhang, Z. Chen, Y. Pan, J. Tang, K. Wu, S.-F. Hung, H. M. Chen, L. Zheng, Q. Lu, X. Yang, B. Xu, H. Xiao, J. Li, D. Wang, Q. Peng, C. Chen, Y. Li, *Nat. Chem.* **2019**, *11*, 222-228; b) A. J. Garza, A. T. Bell, M. Head-Gordon, *ACS Catal.* **2018**, *8*, 1490-1499; c) K. J. P. Schouten, Z. Qin, E. Pérez Gallent, M. T. M. Koper, *J. Am. Chem. Soc.* **2012**, *134*, 9864-9867; d) H. Xiao, T. Cheng, W. A. Goddard, *J. Am. Chem. Soc.* **2016**, *139*, 130-136; e) H. Zhang, P. An, W. Zhou, B. Y. Guan, P. Zhang, J. Dong, X. W. Lou, *Sci. Adv.* **2018**, *4*, eaao6657; f) S. Gao, Z. Sun, W. Liu, X. Jiao, X. Zu, Q. Hu, Y. Sun, T. Yao, W. Zhang, S. Wei, Y. Xie, *Nat. Commun.* **2017**, *8,* 14503; g) Y. Zhu, J. Zheng, J. Ye, Y. Cui, K. Koh, L. Kovarik, D. M. Camaioni, J. L. Fulton, D. G. Truhlar, M. Neurock, C. J. Cramer, O. Y. Gutiérrez, J. A. Lercher, *Nat. Commun.* **2020**, *11,* 5849.

[6] a) M. Ma, K. Djanashvili, W. A. Smith, *Angew. Chem. Int. Ed.* **2016**, *55*, 6680-6684; b) X. Nie, M. R. Esopi, M. J. Janik, A. Asthagiri, *Angew. Chem. Int. Ed.* **2013**, *52*, 2459-2462; c) K. D. Yang, W. R. Ko, J. H. Lee, S. J. Kim, H. Lee, M. H. Lee, K. T. Nam, *Angew. Chem. Int. Ed.* **2017**, *56*, 796-800.

[7] a) B. An, Z. Li, Y. Song, J. Zhang, L. Zeng, C. Wang, W. Lin, *Nat. Catal.* **2019**, *2*, 709-717; b) D. Gao, I. Sinev, F. Scholten, R. M. Arán‐Ais, N. J. Divins, K. Kvashnina, J. Timoshenko, B. Roldan Cuenya, *Angew. Chem. Int. Ed.* **2019**, *58*, 17047-17053.

[8] a) R. M. Arán-Ais, F. Scholten, S. Kunze, R. Rizo, B. Roldan Cuenya, *Nat. Energy* **2020**, *5*, 317-325; b) W. Zhang, C. Huang, Q. Xiao, L. Yu, L. Shuai, P. An, J. Zhang, M. Qiu, Z. Ren, Y. Yu, *J. Am. Chem. Soc.* **2020**, *142*, 11417-11427; c) P.-P. Yang, X.-L. Zhang, F.-Y. Gao, Y.-R. Zheng, Z.-Z. Niu, X. Yu, R. Liu, Z.-Z. Wu, S. Qin, L.-P. Chi, Y. Duan, T. Ma, X.-S. Zheng, J.-F. Zhu, H.-J. Wang, M.-R. Gao, S.-H. Yu, *J. Am. Chem. Soc.* **2020**, *142*, 6400-6408.

[9] Q. Zhu, X. Sun, D. Yang, J. Ma, X. Kang, L. Zheng, J. Zhang, Z. Wu, B. Han, *Nat. Commun.* **2019**, *10,* 3851.

[10] a) J. H. Montoya, C. Shi, K. Chan, J. K. Nørskov, *J. Phys. Chem. Lett.* **2015**, *6*, 2032-2037; b) R. Kortlever, J. Shen, K. J. P. Schouten, F. Calle-Vallejo, M. T. M. Koper, *J. Phys. Chem. Lett.* **2015**, *6*, 4073-4082; c) K. J. P. Schouten, Y. Kwon, C. J. M. van der Ham, Z. Qin, M. T. M. Koper, *Chem. Sci.* **2011**, *2*, 1902-1909; d) K. Jiang, R. B. Sandberg, A. J. Akey, X. Liu, D. C. Bell, J. K. Nørskov, K. Chan, H. Wang, *Nat. Catal.* **2018**, *1*, 111-119.

[11] a) Y.-S. Wei, M. Zhang, R. Zou, Q. Xu, *Chem. Rev.* **2020**, *120*, 12089−12174; b) J. Q. Shen, P. Q. Liao, D. D. Zhou, C. T. He, J. X. Wu, W. X. Zhang, J. P. Zhang, X. M. Chen, *J. Am. Chem. Soc.* **2017**, *139*, 1778-1781; c) L. Zhang, X. X. Li, Z. L. Lang, Y. Liu, J. Liu, L. Yuan, W. Y. Lu, Y. S. Xia, L. Z. Dong, D. Q. Yuan, Y. Q. Lan, *J. Am. Chem. Soc.* **2021**; d) D. H. Nam, O. S. Bushuyev, J. Li, P. De Luna, A. Seifitokaldani, C. T. Dinh, F. P. Garcia de Arquer, Y. Wang, Z. Liang, A. H. Proppe, C. S. Tan, P. Todorovic, O. Shekhah, C. M. Gabardo, J. W. Jo, J. Choi, M. J. Choi, S. W. Baek, J. Kim, D. Sinton, S. O. Kelley, M. Eddaoudi, E. H. Sargent, *J. Am. Chem. Soc.* **2018**, *140*, 11378-11386; e) S. Chen, Z. N. Chen, W. H. Fang, W. Zhuang, L. Zhang, J. Zhang, *Angew. Chem. Int. Ed.* **2019**, *58*, 10932-10935.

[12] a) Y. Zhang, L. Jiao, W. Yang, C. Xie, H.-L. Jiang, *Angew. Chem. Int. Ed.* **2021**, 60, 7607-7611; b) L. Jiao, W. Yang, G. Wan, R. Zhang, X. Zheng, H. Zhou, S. H. Yu, H.-L. Jiang, *Angew. Chem. Int. Ed.* **2020**, 59, 20589-20595; c) Y.-N. Gong, L. Jiao, Y. Qian, C.-Y. Pan, L. Zheng, X. Cai, B. Liu, S. H. Yu, H.-L. Jiang, *Angew. Chem. Int. Ed.* **2020**, 59, 2705-2709; d) Z. Lei, Y. Xue, W. Chen, W. Qiu, Y. Zhang, S. Horike, L. Tang, *Adv. Energy Mater.* **2018**, 8, 1801587; e) P. Shao, L. Yi, S. Chen, T. Zhou, J. Zhang, *J. Energy Chem.* **2020**, 40, 156-170; f) J. Liu, D. Zhu, C. Guo, A. Vasileff, S.-Z. Qiao, *Adv. Energy Mater.* **2017**, 7, 1700518.

[13] a) Q.-L. Hong, H.-X. Zhang, J. Zhang, *J. Mater. Chem. A* **2019**, 7, 17272-17276; b) G. Xu, H. Zhang, J. Wei, H.-X. Zhang, X. Wu, Y. Li, C. Li, J. Zhang, J. Ye, *ACS Nano* **2018**, 12, 5333-5340; c) H.-X. Zhang, Q.-L. Hong, J. Li, F. Wang, X. Huang, S. Chen, W. Tu, D. Yu, R. Xu, T. Zhou, J. Zhang, *Angew. Chem. Int. Ed.* **2019**, 58, 11752-11756; d) M.-R. Liu, Q.-L. Hong, Q.-H. Li, Y. Du, H.-X. Zhang, S. Chen, T. Zhou, J. Zhang, *Adv. Funct. Mater.* **2018**, 28, 1801136; e) T. Wen, Y. Zheng, C. Xu, J. Zhang, M. Jaroniec, S.-Z. Qiao, *Mater. Horiz.* **2018**, 5, 1151-1155.

[14] B. An, Z. Li, Y. Song, J. Zhang, L. Zeng, C. Wang, W. Lin, *Nat. Catal.* **2019**, *2*, 709-717.

[15] W. Ma, S. Xie, T. Liu, Q. Fan, J. Ye, F. Sun, Z. Jiang, Q. Zhang, J. Cheng, Y. Wang, *Nat. Catal.* **2020**, *3*, 478-487

[16] A. M. Abdel-Mageed, B. Rungtaweevoranit, M. Parlinska-Wojtan, X. Pei, O. M. Yaghi, R. J. Behm, *J. Am. Chem. Soc.* **2019**, *141*, 5201-5210.

[17] The X-ray crystallographic coordinates for structures reported in this article have been deposited at the Cambridge Crystallographic Data Centre (CCDC) under deposition numbers CCDC **BIF-102** (2065618), **BIF-103** (2065619) and **BIF-104** (2065620). These data can be obtained free of charge from the Cambridge Crystallographic Data Centre via http://www.ccdc.cam.ac.uk/data_request/cif.

10.1002/anie.202106004

Entry for the Table of Contents

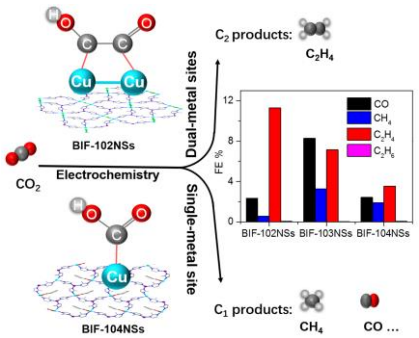

The chemically well-defined catalysts with atomically dispersed dimer-copper sites are elaborated to modulate the reaction path of CO_2 electroreduction reaction (CO_2RR). BIF-102NSs catalyst with Cl^- bridged dimer copper (Cu_2) units shows higher catalytic activity and selectivity for C_2H_4, because the neighboring Cu monomers perform as regulator for varying the reaction barrier and afford distinct reaction paths compared with isolated monomers.